Journal of the Endocrine Society, 2021, Vol. 5, No. 11, 1–11
https://doi.org/10.1210/jendso/bvab154
Clinical Research Article

Clinical Research Article

Efficacy of Differential Diagnosis of Thyroid Nodules by Shear Wave Elastography—the Stiffness Map

Myung Hi Yoo,[1,2] Hye Jeong Kim,[1] In Ho Choi,[3] Suyeon Park,[4,5] Sumi Yun,[6] Hyeong Kyu Park,[1] Dong Won Byun,[1] and Kyoil Suh[1]

[1]Division of Endocrinology and Metabolism, Department of Internal Medicine, Soonchunhyang University Hospital, Soonchunhyang University College of Medicine, Seoul 04401, Korea; [2]Elim Thyroid Clinic, Seoul 06520, Korea; [3]Department of Pathology, Soonchunhyang University Hospital, Seoul 04401, Korea; [4]Department of Biostatics and Data Innovation, Soonchunhyang University, College of Medicine, Seoul 04401, Korea; [5]Department of Applied Statistics, Chung-Ang University, Seoul 06974, Korea; and [6]Department of Diagnostic Pathology, Samkwang Medical Laboratories, Seoul 06742, Korea

ORCiD numbers: 0000-0003-2511-0241 (M. H. Yoo); 0000-0003-1010-9803 (H. J. Kim); 0000-0002-1551-6849 (I. H. Choi); 0000-0002-6391-557X (S. Park); 0000-0003-0086-0679 (S. Yun); 0000-0001-5110-122 (H. K. Park); 0000-0002-1832-7410 (D. W. Byun); 0000-0001-7858-0920 (K. Suh).

Abbreviations: AUC, area under the curve; BSRTC, Bethesda System for Reporting Thyroid Cytopathology; CLT, chronic lymphocytic thyroiditis; CNB, core needle biopsy; D/W, nodule depth/width; EI, elasticity index; FA, follicular adenoma; FN, follicular neoplasm; FNA, fine needle aspiration; FTC, follicular thyroid carcinoma; FVPTC, follicular variant papillary carcinoma; MTC, medullary thyroid carcinoma; NH, nodular hyperplasia; NPV, negative predictive value; PPV, positive predictive value; PTC, papillary thyroid cancer; ROC, receiver operating characteristic; ROI, region of interest; ST, subacute thyroiditis; SWE, shear wave elastography; USG, ultrasonography.

Received: 12 April 2021; Editorial Decision: 22 September 2021; First Published Online: 3 October 2021; Corrected and Typeset: 22 October 2021.

Abstract

Background: Fine needle aspiration is the gold standard for differential diagnosis of thyroid nodules; however, the malignancy rate for indeterminate cytology is 20% to 50%.
Objective: We evaluated the efficacy of shear wave elastography added to ultrasonography for differential diagnosis of thyroid nodules.
Methods: We retrospectively reviewed the medical records of 258 consecutive patients. Thyroid nodules were divided into 4 categories according to maximum elasticity (E_{Max}) and nodule depth/width (D/W) ratio: Category 1 ($E_{Max} \geq 42.6$ kPa; D/W < 0.9); Category 2 ($E_{Max} < 42.6$ kPa; D/W < 0.9); Category 3 ($E_{Max} \geq 42.6$ kPa; D/W ≥ 0.9); and Category 4 ($E_{Max} < 42.6$ kPa; D/W ≥ 0.9). The E_{Max} cutoff value was set using receiver operating characteristic (ROC) curve analysis to predict nodular hyperplasia (NH) vs follicular neoplasm (FN). Cutoff value for nodule D/W ratio was set using ROC curve analysis for malignancy.
Results: NH was the most prevalent pathology group in Category 1, FN in Category 2, and papillary thyroid carcinoma in Category 3. Category 3 demonstrated the highest rate of malignancy (81.8%) and had 55.4% sensitivity and 90% specificity for predicting

ISSN 2472-1972

malignancy. When assessing the benign pathology of NH in follicular patterned lesion, Category 1 demonstrated the highest NH prevalence of 88.9% (34/37) and had 73.9% sensitivity and 85.0% specificity.

Conclusion: The performance for malignancy was highest in Category 3 and predictive ability for benign pathology of NH in follicular lesion was highest in Category 1. The information of E_{Max} and nodule D/W ratio was useful to predict the pathology of thyroid nodules.

Key Words: elastography, shear wave, thyroid nodule, differential diagnosis

Thyroid nodule is a common disease that is found in up to 60% of the population on ultrasound (USG) examination [1, 2] and its malignancy rate is 5% to 15% [3]. Fine needle aspiration (FNA) is the first step in differentiating malignant thyroid nodules. Papillary thyroid carcinoma (PTC), which accounts for 80% to 90% of thyroid cancer, has several characteristic findings on USG and FNA [4-6], which allows for an accurate diagnosis. On the other hand, differential diagnosis of follicular patterned lesions, including nodular hyperplasia (NH), follicular adenoma (FA), follicular thyroid carcinoma (FTC), and follicular variant papillary carcinoma (FVPTC), is challenging because of the lack of distinguishing and overlapping features on FNA [7-9] and USG [10, 11].

According to the Bethesda System for Reporting Thyroid Cytopathology (BSRTC) classification [3] and the 2015 American Thyroid Association guidelines [12] for thyroid nodules in the indeterminate FNA including category III (atypia or follicular lesion of undetermined significance) and category IV (follicular neoplasm or suspicious for follicular neoplasm), diagnostic surgery (lobectomy) is recommended. The malignancy rate of thyroid nodules of indeterminate category has been reported to be in the range of 20% to 50%, resulting in 50% to 80% of patients with unnecessary diagnostic surgery [3, 7, 8, 13-18]. Therefore, additional tools are needed for the further differential diagnosis of thyroid nodules.

USG elastography has been reported to be useful in differentiating benign and malignant thyroid nodules [19-23]. Strain elastography was initially developed for this purpose but had high operator dependence in terms of compression and absence of sufficient quantitative information [24, 25]. Shear wave elastography (SWE) has sufficient quantitative information and is operator-independent in terms of compression, so SWE is more reproducible than strain elastography, and 2-dimensional SWE (2D-SWE) illustrates the focal tissue stiffness map [26, 27]. Thyroid nodules usually show heterogeneous images of elasticity index (EI) within the nodule on 2D-SWE, so the selection of a different location for the region of interest (ROI) within a nodule displays different EI [26, 28]. Recently, we reported that the EI in the total nodular ROI showed higher reproducibility and better agreement in intra- and interrater assay than in the focal nodular ROI, possibly due to the avoidance of the subjective variance of ROI placement in the focal nodular area [29]. In addition, our study showed that EI correlates with the degree of fibrosis, and that the location of fibrosis of surgical pathology is concordant with high EI area on SWE [29].

We aimed to evaluate the efficacy of SWE in the differential diagnosis of follicular patterned lesions, which are the most frequently found entities, comprising more than 50% of FNA [1, 6]. The rate of malignancy of indeterminate follicular lesion (category IV) in diagnostic surgery is 20% to 50% [3, 7, 8, 13-18], resulting in unnecessary diagnostic surgery for 50% to 80% of cases. Additionally, 30% to 50% of benign diagnostic surgery was revealed to be NH [14, 30]. Pathologically, NH shows focal nonneoplastic hyperplasia and subsequent involutional changes accompanied by various degenerative changes, including hemorrhage, infiltration of inflammatory cells, and fibrotic change with incomplete capsule formation [4, 31], while FA is composed of neoplastic cells completely encapsulated and typically shows scanty interstitial tissue [5] and is devoid of degenerative changes [32]. Therefore, the degree and quantity of fibrosis is usually larger in NH than in FA.

A recent application of SWE showed that it was useful in the evaluation of fibrosis, especially in the evaluation of chronic liver disease and liver cirrhosis [33]. Thus, we studied the diagnostic performance of SWE to differentiate follicular neoplasm (FN) from NH in follicular lesions of thyroid nodules [34]. We analyzed the magnitude of EI; the E_{Max}, E_{Mean}, and E_{SD} were significantly lower in the FN than in the NH group ($P < 0.001$) [34].

Our previous study suggested that SWE of thyroid nodules seemed to reflect the degree of fibrosis. Here, we aimed to evaluate the SWE EI in various pathology groups of thyroid nodules and further assessed whether SWE might provide further information when added to the result of B mode USG, especially nodule depth/width (D/W) ratio. We analyzed the patterns of EI and nodule D/W ratio in various pathology groups and evaluated whether SWE might be useful for predicting the histopathology of thyroid nodules.

Methods

Study Population

We retrospectively reviewed the medical records of 258 consecutive patients who visited the thyroid clinic of Soonchunhyang University Hospital (between August 2016 and May 2020, n = 224) and the Elim Thyroid Clinic (between March 2019 and May 2020, n = 34) for the evaluation of thyroid nodules and who underwent SWE before USG-guided FNA and/or core needle biopsy (CNB). According to the American [12] and Korean [35] management guidelines for patients with thyroid nodules, the FNA and/or CNB criteria for thyroid nodules are as follows: (1) USG findings show a nodule that can be classified as malignant with characteristics such as microcalcifications, hypoechogenicity, irregular margins, or a taller-than-wide shape > 1.0 cm in diameter; and (2) indeterminate findings on USG show a nodule > 1.5 cm in diameter.

Thirty-three thyroid nodules were excluded because, based on the BSRTC [36], they were characterized as nondiagnostic or unsatisfactory (n = 21) or atypia of undetermined significance (n = 12). To avoid artifacts by SWE, thyroid nodules with poor shear wave mapping (n = 15) or thyroid nodules including macrocalcifications (n = 7) and in the isthmic/paraisthmic areas due to the interference produced by the tracheal cartilage (n = 18) were excluded. Therefore, 185 patients were included for the study. After the evaluation of the diagnostic efficacy of maximum elasticity (E_{Max}) combined with the nodule D/W ratio, an additional 40 patients (5 with subacute thyroiditis, 11 with nodular hyperplasia, 4 with chronic lymphocytic thyroiditis, 7 with follicular neoplasm, and 13 with papillary thyroid carcinoma) were excluded for diffuse pattern of the lesion or ill-defined margin or lack of the measurement of the both diameters or diagonal measurement of the diameter. Ultimately, 145 patients were included in the last evaluation. The study design was approved by the ethics review board of the Soonchunhyang University Hospital.

Gray-Scale USG and SWE Examinations

The patients were positioned for the USG with their necks extended. Each patient underwent gray-scale USG and SWE before USG-guided FNA and/or CNB. Ultrasonography was performed using the Aixplorer USG system (SuperSonic Imagine, Aix-en-Provence, France), with a 15–4 MHz linear probe, by 2 experienced endocrinologists specializing in the thyroid. Each thyroid nodule was scanned in the longitudinal and transverse planes.

During gray-scale USG examination, thyroid nodules were described according to the internal contents, echogenicity, shape, margin, calcifications, central vascularity, peripheral halo, size (width, depth, and length), and volume. After the gray-scale USG, SWE was executed by the same operator who performed the gray-scale USG, using the same probe. To avoid compression artifacts, a generous amount of gel was used. The probe was held static in the transverse plane at the center of the nodule until the image stabilized. After acquiring 2 or 3 cine-loop images, 1 representative elastogram was selected with the fewest artifacts in each cine-loop image. The software automatically calculated shear elasticity indices (EI) in the ROI as the mean (E_{Mean}), minimum (E_{Min}), maximum (E_{Max}), and standard deviation (E_{SD}) in kilopascals (kPa).

USG-Guided FNA and CNB Procedures

USG-guided FNA procedures were performed using 21- to 23-gauge needles attached to a 10-mL syringe. USG-guided CNB procedures were performed under local anesthesia with 1% lidocaine and using a disposable 18-gauge, double-action spring-activated needle (TSK Ace-cut, Create Medic, Yokohama, Japan). Using a free hand technique, the tip of the biopsy needle was manually advanced to the margin of the nodule, and the stylet and cutting cannula of the needle were sequentially fired. The procedure was continuously monitored using USG. FNA and CNB were performed as described before [29].

Pathological Analysis

FNA cytology was diagnosed according to the BSRTC [3]. Diagnostic categories of thyroid CNB were divided according to the criteria reported by the Korean Endocrine Pathology study group [37]: category I (nondiagnostic); category II (benign lesion including benign follicular nodule, NH); category IIIA (indeterminate follicular lesions with nuclear atypia); category IIIB (indeterminate follicular lesion with architectural atypia, including microfollicular lesions, solid, or trabecular follicular lesions, and Hürthle cell proliferative lesions lacking a fibrous capsule); category IV (FN/suspicious for FN showing category IIIB lesion with a fibrous capsule); category V (suspicious for malignancy); and category VI (malignant). The endocrine pathologist (I. H. Choi) reviewed all CNB slides and CNB category II was grouped as suggestive of NH, and CNB category IIIB and IV were grouped as suggestive of FN. Surgical histopathology was diagnosed according to the World Health Organization (WHO) classification [5].

Statistical Analysis

The elasticity values of all lesions were expressed as medians (25th, 75th percentile), and the differences between

groups were compared using one-way analysis of variance (ANOVA), Tukey's multiple comparison test and Kruskal-Wallis test and pairwise test for multiple comparisons of mean rank sums (Dunn's test) with Bonferroni correction.

Group comparisons of categorical variables were performed using the χ^2 test or (for small cell values) the Fisher's exact test and Bonferroni's correction. The results of the categorical data area were summarized using frequencies and percent values. We evaluated the sensitivity and specificity of the E_{Max} value to predict FN and also of the nodule D/W ratio to differentiate malignant nodules from benign nodules using receiver operating characteristic (ROC) curve analyses and estimating the area under the curve (AUC) with 95% CI. All statistical analyses were performed using the IBM SPSS Statistics 26.0 software package (Chicago, IL, USA) and $P < 0.05$ was considered statistically significant.

Results

EI on SWE in Various Pathology Groups

FN showed the lowest E_{Max} among all pathologies and FN showed lower E_{Max} than the NH, PTC, and subacute thyroiditis (ST) groups ($P < 0.05$, Fig. 1, Fig. 2). The ST group had the highest EI of all pathology groups (Table 1, Fig. 1), and ST showed higher E_{Max} than chronic lymphocytic thyroiditis (CLT), NH, FN, and PTC ($P < 0.01$, Fig. 1). PTC showed a higher E_{Mean} than nonconventional PTC ($P < 0.05$, Fig. 1).

Analysis of the Distribution of EI in Pathology Groups

The EI distribution was analyzed in 4 pathology groups (CLT, FN, NH, and PTC), excluding other groups that included smaller numbers less than 10. Results of a Kruskal-Wallis test followed by pairwise test for multiple comparisons of mean rank sums (Dunn's test) showed statistically significant difference of E_{Max} between FN vs NH and FN vs PTC and statistically significant difference of E_{Mean} between FN vs CLT, FN vs NH, and FN vs PTC (Fig. 1, Fig. 3; $P < 0.001$). Analysis of distribution patterns of E_{Max} in the pathology groups showed that E_{Max} in FN was significantly lower than in NH and PTC but there was no significant difference of E_{Max} among CLT, NH, and PTC (Fig. 1, Fig. 3), suggesting that additional parameters would be needed for further differential diagnosis among CLT, NH, and PTC.

Diagnostic Performance of E_{Max} to Detect FN and Nodule Depth/Width Ratio to Detect Malignancy

The ROC analysis and diagnostic accuracy of the E_{Max} for discrimination between NH and FN are shown in Fig. 4. An E_{Max} level of 42.6 kPa was the optimal cutoff value with sensitivity of 84.8%, specificity of 84.9%, diagnostic accuracy of 86.3%, and the AUC was 0.934 (Fig. 4A). The ROC analysis and diagnostic accuracy of the nodule D/W ratio for the differentiation of the malignant nodules from benign nodules are presented in Fig. 4B. The optimal cutoff

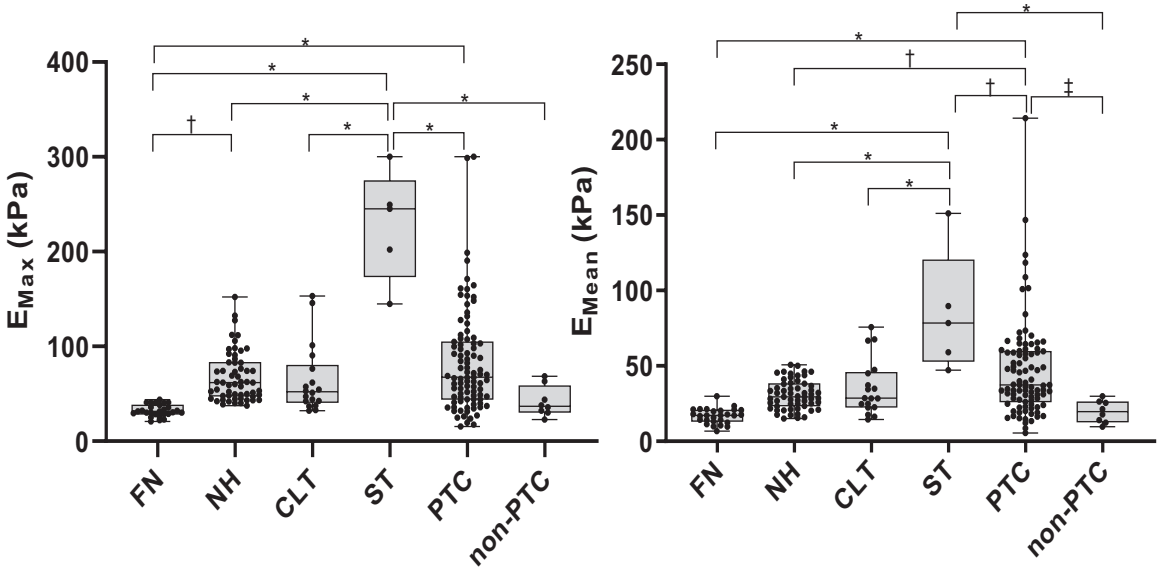

Figure 1. Box-and-whisker plots of elasticity index measurements on shear wave elastography according to thyroid nodule pathology. Abbreviations: E_{Mean}, mean elasticity; E_{Max}, maximum elasticity values; kPa, kilopascal; FN, follicular neoplasm (n = 27); NH, nodular hyperplasia (n = 57); CLT, chronic lymphocytic thyroiditis (n = 18); ST, subacute thyroiditis (n = 5); PTC, papillary thyroid carcinoma (n = 70); non-PTC, nonconventional papillary thyroid carcinoma including follicular variant of papillary thyroid carcinoma (n = 2), follicular thyroid carcinoma (n = 4), and medullary thyroid carcinoma (n = 3). *$P < 0.001$, †$0.001 \le P < 0.01$, ‡$0.01 \le P < 0.05$.

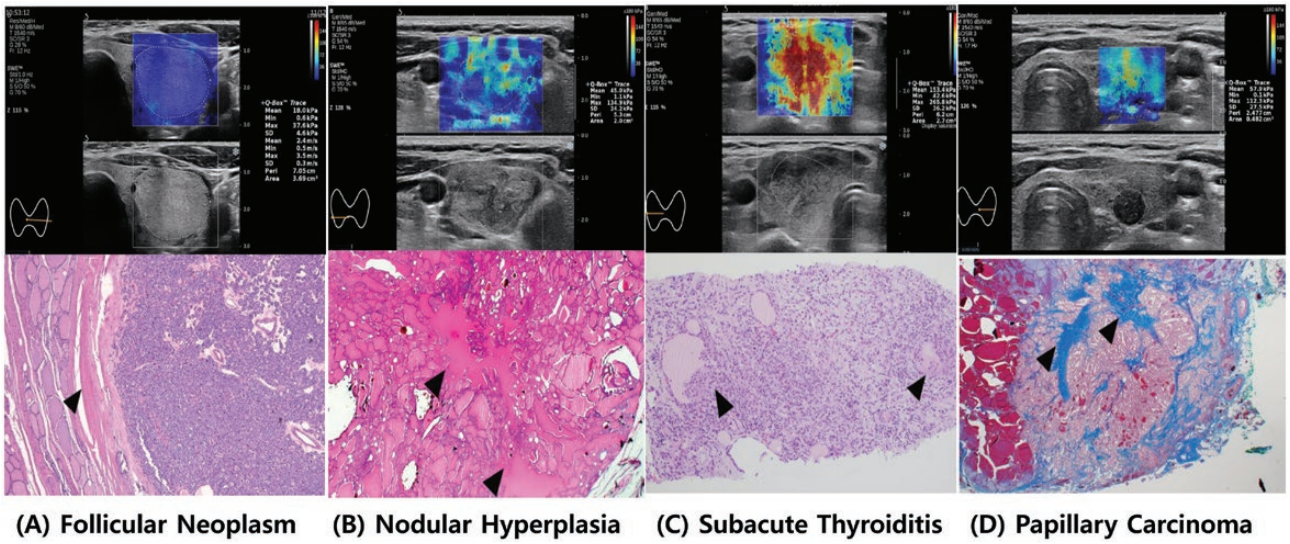

Figure 2. Shear wave elastography (SWE), gray-scale ultrasound, and hematoxylin and eosin (H&E) staining or Masson's trichrome staining of the histopathology of the thyroid nodule in 4 patients. A, Follicular adenoma SWE showed low elasticity index (EI), which was color-coded as deep blue. Histopathology showed that abortive microfollicles were well encapsulated (arrow) and scanty amount of interstitial tissue with little fibrosis causing low EI on SWE. B, Nodular hyperplasia SWE showed areas of elevated EI, which is color-coded as light blue, yellow to red and showed the pattern of high elasticity as traversing the nodule. Histopathology showed micro- and macrofollicles with interstitial fibrosis (arrow) causing scattered high EI on SWE. C, Subacute thyroiditis SWE showed highest EI, which is color-coded as red in hypoechoic geographic nodule with irregular margin. Core needle biopsy showed granulomatous thyroiditis with epithelial cells and giant cells (arrow). D, Papillary thyroid carcinoma (PTC) SWE showed elevated areas of EI, which is color-coded as yellow and red in the upper region of the thyroid nodule. Surgical pathology with Masson-trichrome stain showed PTC with fibrosis in the upper portion of the nodule (arrow), which matched the high EI area, color-coded as yellow and red on SWE.

value for nodule D/W ratio was 0.90, with sensitivity of 69.6%, specificity of 83.8%, diagnostic accuracy of 77.9%, and the AUC was 0.801 (Fig. 4B).

Distribution Patterns of the Pathology Groups in Each Category

Thyroid nodules were divided into 4 groups according to E_{Max} and nodule depth/width (D/W) ratio (Fig. 5): Category 1 ($E_{Max} \geq 42.6$ kPa; D/W < 0.9); Category 2 ($E_{Max} < 42.6$ kPa; D/W < 0.9); Category 3 ($E_{Max} \geq 42.6$ kPa; D/W ≥ 0.9); and Category 4 ($E_{Max} < 46.2$ kPa; D/W ≥ 0.9).

Category 1 was composed of NH (55.7%), PTC (23%), and CLT (13.1%) (Table 2, Fig. 5). Category 2 was composed of FN (48.3%), NH (17.2%), non-PTC (13.8%), PTC (10.3%) and CLT (10.3%). Category 3 was composed of PTC (75.0%), NH (11.4%), CLT (6.8%), and non-PTC (6.8 %). Category 4 was composed of PTC (54.6%), FN (27.3%), and NH (18.2%) (Table 2, Fig. 5). The distribution patterns of the pathology groups in the 4 categories showed statistically significant difference between the Category 1 vs 2, the Category 1 vs 3, and the Category 2 vs 3 by Fisher's exact test and Bonferroni correction ($P < 0.001$).

We found that NH was the most prevalent pathology group in Category 1 (Fig. 5, Fig. 6), FN was the most prevalent pathology group in Category 2, and PTC was the most prevalent pathology group in the categories 3 and 4 (Fig. 6).

Predictive Ability of Each Category for Malignancy

When evaluating the performance of each category defined by E_{Max} (42.6 kPa) and nodule D/W ratio on predicting malignancy, the Category 3 demonstrated the highest rate of malignancy (81.8%) and had 55.4% sensitivity and 90% specificity, 81.2% positive predictive value (PPV) and 71.3% negative predictive value (NPV) (Table 3).

Performance of E_{Max} (42.6 kPa) and D/W Ratio (0.9) for Differentiating NH From FN in Follicular Patterned Lesions by FNA

When assessing the utility of each category in differentiating NH from FN in follicular patterned lesions by FNA, the Category 1 demonstrated the highest NH prevalence of 88.9% (34/37) and had a sensitivity of 73.9% and a specificity of 85.0%, a PPV of 91.9% and a NPV of 58.6% (Table 4).

Discussion

SWE assesses tissue stiffness (fibrosis > carcinoma > glandular tissue > fat) [38] and creates a map of stiffness [39, 40]. Regarding thyroid nodules, several studies have reported that elasticity is correlated with the degree of fibrosis and not with cell number or cell density [41-43]. Rago et al

Table 1. Elasticity index (kPa) on shear wave elastography according to the thyroid nodule pathology

Pathology	E_{Mean}	E_{Min}	E_{Max}	E_{SD}
FN (n = 27)	17.2 (13.7, 20.6)	3.6 (1.5, 8.2)	31.5 (28.8, 37.1)	5.6 (3.7, 6.1)
NH (n = 57)	29.5 (23.5, 38.0)	8.9 (2.0, 14.2)	61.7 (47.8, 82.9)	9.6 (7.5, 13.1)
CLT (n = 18)	28.6 (22.7, 45.2)	7.9 (1.8, 20.0)	52.0 (42.0, 76.5)	8.2 (6.0, 14.8)
ST (n = 5)	78.4 (59.0, 89.6)	4.4 (1.5, 5.1)	245.3 (202.1, 249.5)	39.3 (38.2, 56.4)
PTC (n = 70)	37.3 (26.6, 59.3)	15.5 (2.7, 28.9)	67.4 (45.3, 103.9)	11.2 (6.3, 19.2)
FVPTC (n = 2)	22.0 (14.1, 29.8)	11.1 (4.0, 18.2)	39.9 (35.8, 43.9)	NA
FA (n = 7)	14.0 (12.4, 15.5)	1.1 (0.8, 6.2)	32.0 (26.9, 39.5)	6.0 (4.8, 7.5)
HCA (n = 4)	10.7 (8.7, 16.0)	1.6 (0.4, 5.3)	28.6 (25.1, 31.2)	3.8 (3.1, 5.1)
FTC (n = 4)	17.9 (13.8, 19.7)	2.6 (2.5, 8.3)	30.0 (26.4, 31.1)	4.9 (3.6, 5.0)
MTC (n = 3)	25.6 (19.0, 26.0)	3.1 (1.6, 8.3)	63.2 (50.6, 65.8)	8.9 (8.8, 10.7)

Data are presented as median and interquartile range; 25th and 75th percentiles.
Abbreviations: CLT, chronic lymphocytic thyroiditis; E_{Max}, maximum elasticity; E_{Mean}, mean elasticity; E_{Min}, minimum elasticity; E_{SD}, 1 standard deviation of elastographic values; FA, follicular adenoma; FN, follicular neoplasm; FTC, follicular thyroid carcinoma; FVPTC, follicular variant of papillary thyroid carcinoma; HCA, Hürthle cell adenoma; NH, nodular hyperplasia; MTC, medullary thyroid carcinoma; PTC, papillary thyroid carcinoma; ST, subacute thyroiditis.

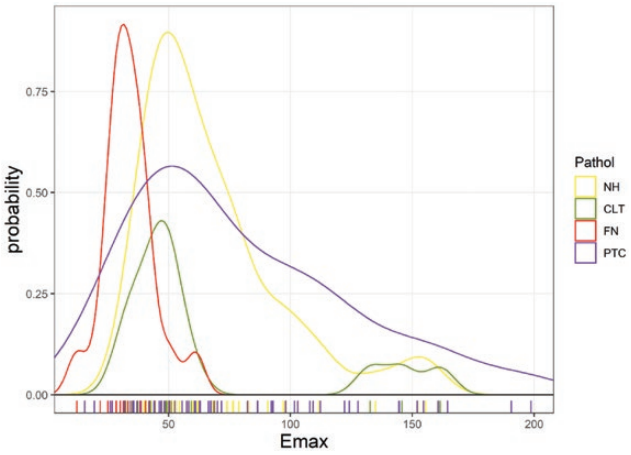

Figure 3. Graph showing distribution of shear wave elasticity (E_{Max}) in various pathology groups. Distribution patterns of E_{Max} in the pathology groups showed statistically significant difference between FN vs NH, and FN vs PTC ($P < 0.001$) but there was no significant difference among CLT, NH, and PTC. Abbreviations: CLT, chronic lymphocytic thyroiditis, FN, follicular neoplasm; NH, nodular hyperplasia; PTC, papillary thyroid carcinoma.

reported that thyroid nodule stiffness was correlated with fibrosis [41] and Yi et al reported that elasticity of papillary thyroid carcinoma was correlated with the fibrosis degree [42]. Fukuhara et al reported that fibrosis played an important role in determining stiffness as measured by shear wave velocity in thyroid and that shear wave velocity was only mildly influenced by high cellular density [44]. Recently, we reported that the EI of thyroid nodules correlates with the degree of fibrosis, and the location of fibrosis in surgical histopathology is concordant with the degree and location of high EI area on SWE [29]. In addition, we had reported that the EI of FN is significantly lower than NH, and that FN shows a high elasticity area only around the capsule (marginal pattern), while NH shows a high EI area traversing the entire nodule [34, 45].

Our data suggested that the characteristic EI pattern of each pathology group probably reflected the degree of fibrosis in each pathology group (Fig. 1, Fig. 2). As expected from the histopathology of the scanty amount of interstitial tissue in FN, FN showed the lowest EI (Table 1, Fig. 1). FN was mainly distributed in the Category 2 (70%) and Category 4 (15%) and both categories were showing E_{Max} < 42.6 kPa. FN showed lower E_{Max} than NH (Fig. 1), in accordance with our previous report [34].

Regarding thyroid carcinoma, PTC showed higher E_{Mean} than the nonconventional PTC group (including FVPTC, FTC, and medullary thyroid carcinoma [MTC]), reflecting the fact that most PTC is usually accompanied by various degrees of fibrosis on histopathology while the nonconventional PTC group showed little fibrosis (Fig. 1). MTC is known to show deposition of amyloid substance but not fibrosis. In our study, 2 of 3 cases of MTC showed only slight elevation of E_{Max} and belonged to Category 1. Thus, different degrees and patterns of tissue fibrosis in

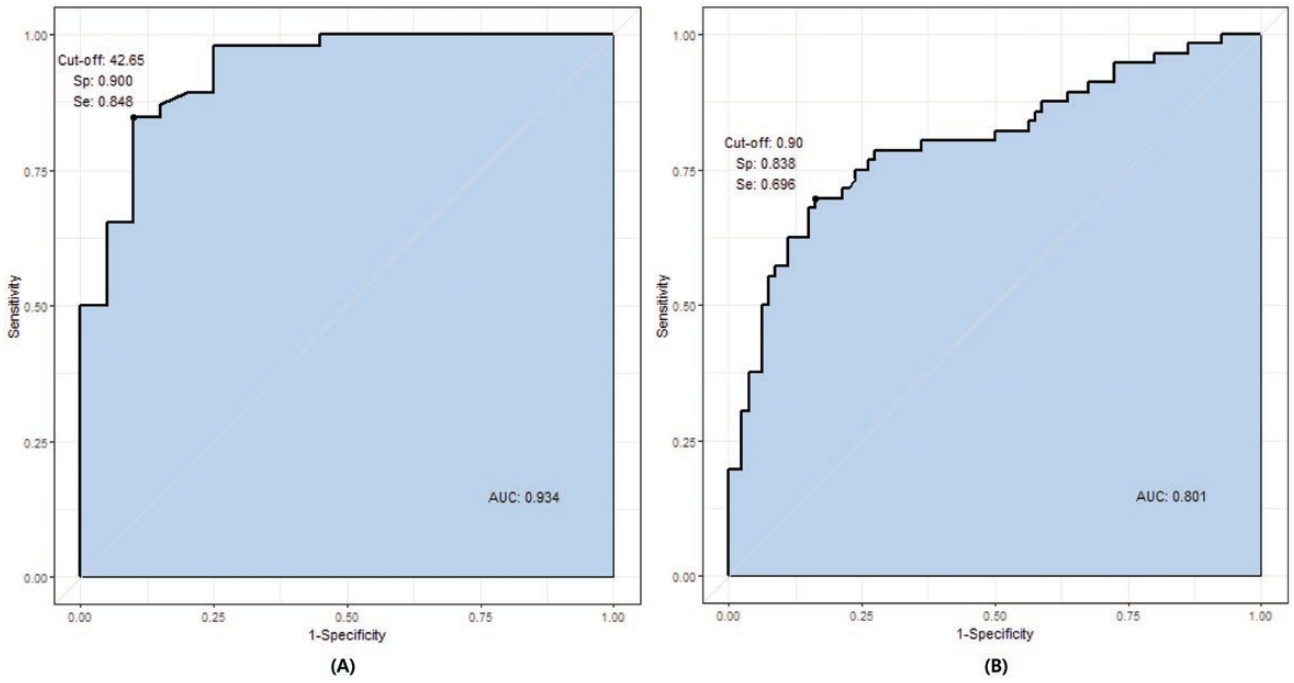

Figure 4. Receiver operating characteristic (ROC) curve of E_{Max} to differentiate follicular neoplasm from nodular hyperplasia (A), and ROC of nodule depth/width ratio to differentiate malignant nodules from benign nodules (B). Abbreviations: AUC, area under the curve; E_{Max} maximum elasticity.

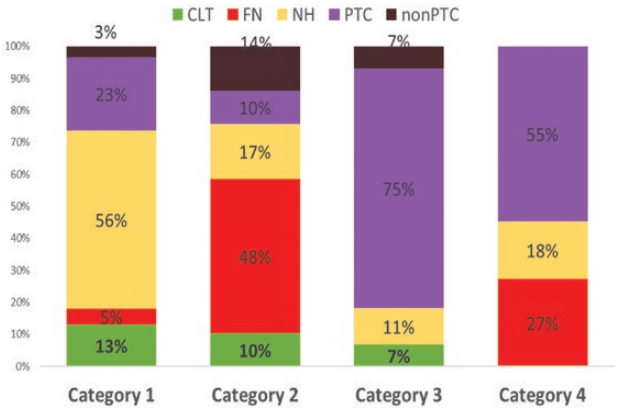

Figure 5. Distribution of the pathology groups in the categories defined by E_{Max} and nodule depth/width ratio (D/W) of the thyroid nodules. Distribution patterns of the pathology groups in the different categories showed statistically significant difference between Category 1 vs 2, Category 1 vs 3, and Category 2 vs 3 by Fisher's exact test and Bonferroni correction ($P < 0.001$). Abbreviations: CLT, chronic lymphocytic thyroiditis; FN, follicular neoplasm; NH, nodular hyperplasia; PTC, papillary thyroid carcinoma; non-PTC nonconventional papillary thyroid carcinoma.

the pathology groups seemed to cause different patterns of elasticity in SWE and characteristic distribution of the pathology groups among the 4 categories (Figs. 5 and 6).

When predicting the malignancy, Category 3 showed the highest prevalence of malignancy and had a sensitivity of 55.4%, a specificity of 90%, a PPV of 81.2%, and a NPV of 71.3% (Table 3) for malignancy, probably due to the increased incidence of fibrosis of PTC resulting in more frequent distribution of PTC in Category 3 compared with Category 4.

Clinically, diagnostic surgery is usually performed for Bethesda category III or IV nodules, which have a rate of malignancy of 30% to 40%, resulting in surgery for benign nodules in more than 50% of cases. Recently Yang et al [46] reported that USG grading using American Thyroid Association, Korean, and American College of Radiology Thyroid Imaging Reporting and Data System (TIRADS) systems were not helpful in stratifying malignancy nor in predicting benign pathology showing sensitivity of 20% to 50% and specificity of 50% to 80% in Bethesda category 4 nodules. Usually, the most frequent pathology of benign diagnostic surgery is NH [14, 30]. Thus, differentiating NH from FN in follicular lesions (which includes Bethesda category IV) will decrease the benign diagnostic surgery of NH. Thus, we tried to evaluate the utility of the category defined by E_{Max} (42.6 kPa) and D/W (0.9) to differentiate NH from FN in follicular lesion, because NH showed higher E_{Max} than FN due to the higher degree of fibrosis on pathology.

To assess the predictive ability of each category for the benign pathology of NH in follicular patterned lesion by FNA, performance of each category defined by E_{Max} (42.6 kPa) and D/W (0.9) for differentiating NH from FN was evaluated by assessing sensitivity, specificity, PPV, and NPV. When evaluating the predicting ability for benign pathology of NH in follicular patterned lesion by FNA, Category 1

Table 2. Distribution of the pathology groups according to the categories defined by E_{Max} and nodule depth/width ratio (D/W) of the thyroid nodules

	Category 1	Category 2	Category 3	Category 4
	E_{Max} ≥ 42.6 kPa & D/W < 0.9	E_{Max} < 42.6 kPa & D/W < 0.9	E_{Max} ≥ 42.6 kPa & D/W ≥ 0.9	E_{Max} < 42.6 kPa & D/W ≥ 0.9
CLT	8 (13.11%)	3 (10.34%)	3 (6.82%)	0 (0%)
FN	3 (4.92%)	14 (48.28%)	0 (0%)	3 (27.27%)
NH	34 (55.74%)	5 (17.24%)	5 (11.36%)	2 (18.18%)
PTC	14 (22.95%)	3 (10.34%)	33 (75%)	6 (54.55%)
Non-PTC	2 (3.28%)	4 (13.79%)	3 (6.82%)	0 (0%)
Total	61(100%)	29 (100%)	44(100%)	11 (100%)

Data are presented as numbers (percentages). Distribution patterns of the pathology groups in the 4 categories showed statistically significant difference between Category 1 vs 2, Category 1 vs 3, and Category 2 vs 3 by Fisher's exact test (P < 0.001).

Abbreviations: E_{Max}, maximum elasticity; FN, follicular neoplasm; NH, nodular hyperplasia; CLT, chronic lymphocytic thyroiditis; PTC, papillary thyroid carcinoma; non-PTC nonconventional papillary thyroid carcinoma including follicular variant of papillary thyroid carcinoma (n = 2), follicular thyroid carcinoma (n = 4), and medullary thyroid carcinoma (n = 3).

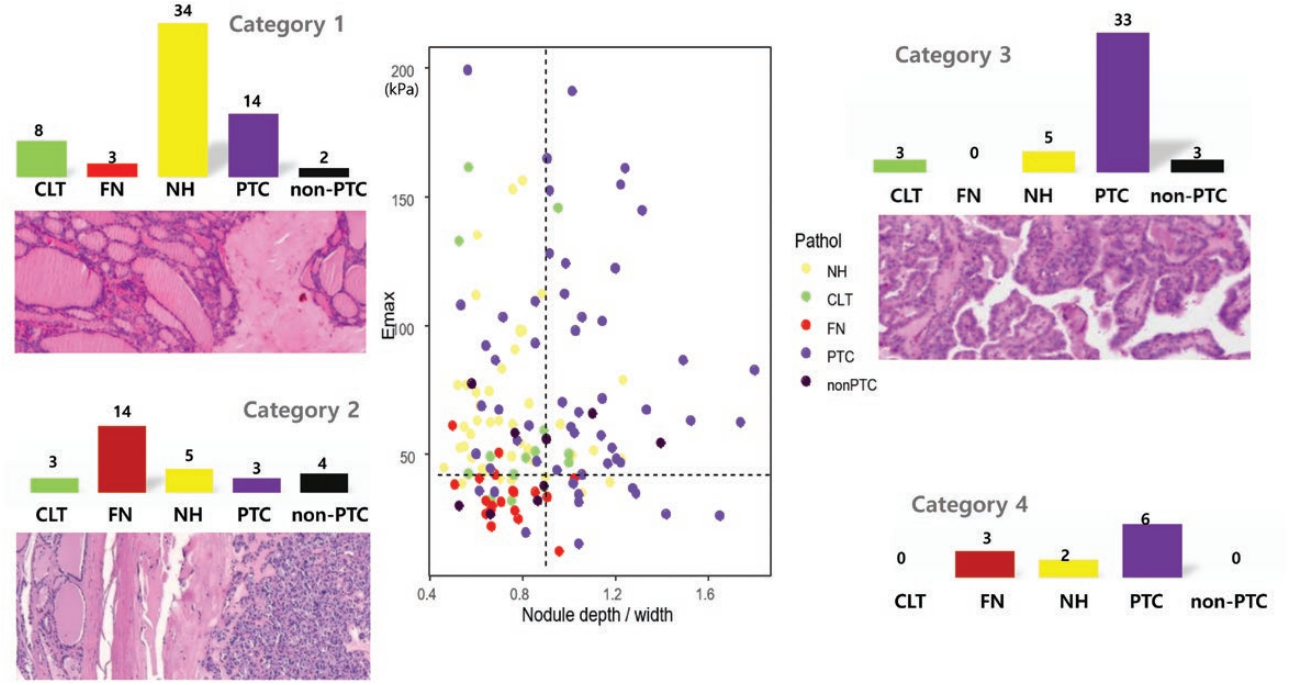

Figure 6. Distribution of the pathology groups according to the categories defined by E_{Max} and nodule depth/width ratio (D/W) of the thyroid nodules. Distribution patterns of the pathology groups showed statistically significant difference between Category 1 vs 2, Category 1 vs 3, and Category 2 vs 3 by Fisher's exact test and Bonferroni correction ($P < 0.001$), illustrating the most prevalent pathology was NH in Category 1, FN in Category 2, and PTC in Category 3.

demonstrated highest prevalence of NH, reflecting the higher degree of fibrosis in NH compared with FN, with higher E_{Max} and more prevalent NH in Category 1 compared with Category 2 (Fig. 5). Category 1 had a sensitivity of 73.9% and a specificity of 85.0%, a PPV of 91.9%, and a NPV of 58.6% (Table 4) for differentiating NH from FN in follicular patterned lesion by FNA. Furthermore, the higher prevalence of FN in Category 2 (E_{Max} < 42.6 kPa) than in Category 1 (E_{Max} ≥ 42.6 kPa) may reflect a lesser degree of fibrosis in FN compared with NH. These points would be helpful to detect NH and avoid diagnostic surgery of NH in follicular patterned lesion, especially in Bethesda category 4.

A limitation of the SWE assessment of thyroid is that the SWE image is influenced by several factors that may constrain its use in clinical practice. Artifacts can occur when the location of the nodules is near the trachea or carotid artery, and nodules that are located deep from the skin may result in poor SWE image. In addition, poor SWE image

Table 3. Predictive ability of each category defined by E_{Max} (42.6 kPa) and D/W ratio (0.9) for malignancy

	Malignancy (%)	Sensitivity (%)	Specificity (%)	PPV (%)	NPV (%)
Category 1 (E_{Max} ≥ 42.6 kPa & D/W < 0.9)	26.2 [16/61]	24.6 (14.7-36.9)	43.8 (32.7-55.3)	26.2 (15.8-39.1)	41.7 (31.0-52.9)
Category 2 (E_{Max} < 42.6 kPa & D/W < 0.9)	24.1 [7/29]	10.8 (4.4-20.9)	72.5 (61.4-81.9)	24.1 (10.3-43.5)	50.0 (40.6-59.4)
Category 3 (E_{Max} ≥ 42.6 kPa & D/W ≥ 0.9)	81.8 [36/44]	55.4 (42.5-67.7)	90.0 (81.2-95.6)	81.2 (67.3-91.8)	71.3 (61.4-80.0)
Category 4 (E_{Max} < 42.6 kPa & D/W ≥ 0.9)	54.5 [6/11]	9.2 (3.46-19.0)	93.8 (86.0-97.9)	54.6 (23.4-83.3)	56.0 (47.2-64.5)

Numbers in parentheses are 95% CIs and numbers in brackets are the data used to calculate percentages.
Abbreviations: D/W, nodule depth/width; E_{Max}, maximum elasticity; NPV, negative predictive value; PPV, positive predictive value.

Table 4. Performance of E_{Max} (42.6 kPa) and D/W ratio (0.9) for differentiating nodular hyperplasia from follicular neoplasm in follicular patterned lesions by fine needle aspiration cytology

	NH	FN	Sensitivity (%)	Specificity (%)	PPV (%)	NPV (%)
Category 1 (E_{Max} ≥ 42.6 kPa & D/W < 0.9)	34	3	73.9 (58.9-85.7)	85.0 (62.1-96.8)	91.9 (78.1-98.3)	58.6 (38.9-76.5)
Category 2 (E_{Max} < 42.6 kPa & D/W < 0.9)	5	14	10.9 (3.6-23.6)	30.0 (11.9-54.3)	26.3 (9.2-5.1)	12.8 (4.8-25.7)
Category 3 (E_{Max} ≥ 42.6 kPa & D/W ≥ 0.9)	5	0	10.9 (3.6-23.6)	100 (83.2-100)	100 (47.8-100)	32.8 (21.3-46.0)
Category 4 (E_{Max} < 42.6 kPa & D/W ≥ 0.9)	2	3	4.4 (0.5-14.8)	85.0 (62.1-96.8)	40.0 (5.3-85.3)	27.9 (17.2-40.8)

Numbers in parentheses are 95% CIs.
Abbreviations: D/W, nodule depth/width; E_{Max}, maximum elasticity; FN, follicular neoplasm; NH, nodular hyperplasia; NPV, negative predictive value; PPV, positive predictive value.

may occur in mixed nodules with cystic fluid, which slows down the speed of the shear wave, and SWE image quality may be reduced in nodules with rim calcification. A limitation of our study is the small size of the sample, especially non-PTC cases. Future studies with larger sample sizes will be needed to address further information, especially regarding non-PTC.

In conclusion, elasticity of SWE may reflect the degree of fibrosis and this information is helpful for the differential diagnosis of thyroid nodules, especially between follicular neoplasm and nodular hyperplasia, and also for the detection of papillary carcinoma, which is frequently accompanied by fibrosis. The performance for malignancy was highest in Category 3 and predictive ability for benign pathology of NH in follicular lesion was highest in Category 1. The information of E_{Max} and nodule D/W ratio was useful to predict the probability of the pathology of thyroid nodules and has the advantages of noninvasiveness, simplicity (no need for great skill), and low cost.

Acknowledgments

We thank Ms. Ha Yul Lee, B.S., for her assistance in preparing the manuscript, and Mi Soon Lim, B.S., Dong Won Shin, B.S., and Sang Keun Hyon, B.S., for their excellent work on the literature survey.

Additional Information

Correspondence: Myung Hi Yoo, M.D., Ph.D., Division of Endocrinology and Metabolism, Department of Internal Medicine, Soonchunhyang University Hospital, Soonchunhyang University College of Medicine, 59 Daesagwan-ro, Yongsan-gu, 140-743, Seoul, Republic of Korea. Email: elimyoo11@gmail.com; mhyoo@schmc.ac.kr.

Disclosures: The authors declare that no conflicts of interest to disclose.

Data Availability: All data generated or analyzed during this study are included in this published article or in the data repositories listed in References.

References

1. Bongiovanni M, Spitale A, Faquin WC, Mazzucchelli L, Baloch ZW. The Bethesda system for reporting thyroid cytopathology: a meta-analysis. *Acta Cytol*. 2012;**56**(4):333-339.
2. Mazzaferri EL. Management of a solitary thyroid nodule. *N Engl J Med*. 1993;**328**(8):553-559.
3. Cibas ES, Ali SZ. The 2017 Bethesda system for reporting thyroid cytopathology. *Thyroid*. 2017;**27**(11):1341-1346.
4. Kumar V, Abbas AK, Aster JC. *Robbins and Cotran Pathologic Basis of Disease*. 9th ed. Philadelphia, PA: Saunders Elsevier; 2015.
5. Lloyd RV, Osamura RY, Kloppel G, Rosai J. *WHO Classification of Tumours of Endocrine Organs (Medicine)*. 4th ed. Lyon, France: International Agency for Research on Cancer; 2017.
6. Ali SZ, Cibas ES. *The Bethesda System for Reporting Thyroid Cytopathology Definitions, Criteria and Explanatory Notes*. New York, NY: Springer; 2010.
7. Alexander EK. Approach to the patient with a cytologically indeterminate thyroid nodule. *J Clin Endocrinol Metab*. 2008;**93**(11):4175-4182.
8. Greaves TS, Olvera M, Florentine BD, et al. Follicular lesions of thyroid: a 5-year fine-needle aspiration experience. *Cancer*. 2000;**90**(6):335-341.
9. Maruta J, Hashimoto H, Suehisa Y, et al. Improving the diagnostic accuracy of thyroid follicular neoplasms: cytological features in fine-needle aspiration cytology. *Diagn Cytopathol*. 2011;**39**(1):28-34.
10. Jeh SK, Jung SL, Kim BS, Lee YS. Evaluating the degree of conformity of papillary carcinoma and follicular carcinoma to the reported ultrasonographic findings of malignant thyroid tumor. *Korean J Radiol*. 2007;**8**(3):192-197.
11. Sillery JC, Reading CC, Charboneau JW, Henrichsen TL, Hay ID, Mandrekar JN. Thyroid follicular carcinoma: sonographic features of 50 cases. *AJR Am J Roentgenol*. 2010;**194**(1):44-54.
12. Haugen BR, Alexander EK, Bible KC, et al. 2015 American Thyroid Association Management Guidelines for Adult Patients with Thyroid Nodules and Differentiated Thyroid Cancer: The American Thyroid Association Guidelines Task Force on Thyroid Nodules and Differentiated Thyroid Cancer. *Thyroid*. 2016;**26**(1):1-133.
13. Marhefka GD, McDivitt JD, Shakir KM, Drake AJ 3rd. Diagnosis of follicular neoplasm in thyroid nodules by fine needle aspiration cytology: does the result, benign vs. suspicious for a malignant process, in these nodules make a difference? *Acta Cytol*. 2009;**53**(5):517-523.
14. Baloch ZW, Fleisher S, LiVolsi VA, Gupta PK. Diagnosis of "follicular neoplasm": a gray zone in thyroid fine-needle aspiration cytology. *Diagn Cytopathol*. 2002;**26**(1):41-44.
15. Yeh MW, Demircan O, Ituarte P, Clark OH. False-negative fine-needle aspiration cytology results delay treatment and adversely affect outcome in patients with thyroid carcinoma. *Thyroid*. 2004;**14**(3):207-215.
16. Bohacek L, Milas M, Mitchell J, Siperstein A, Berber E. Diagnostic accuracy of surgeon-performed ultrasound-guided fine-needle aspiration of thyroid nodules. *Ann Surg Oncol*. 2012;**19**(1):45-51.
17. Carling T, Udelsman R. Follicular neoplasms of the thyroid: what to recommend. *Thyroid*. 2005;**15**(6):583-587.
18. Yoon RG, Baek JH, Lee JH, et al. Diagnosis of thyroid follicular neoplasm: fine-needle aspiration versus core-needle biopsy. *Thyroid*. 2014;**24**(11):1612-1617.
19. Gregory A, Bayat M, Kumar V, et al. Differentiation of benign and malignant thyroid nodules by using comb-push ultrasound shear elastography: a preliminary two-plane view study. *Acad Radiol*. 2018;**25**(11):1388-1397.
20. Veyrieres JB, Albarel F, Lombard JV, et al. A threshold value in shear wave elastography to rule out malignant thyroid nodules: a reality? *Eur J Radiol*. 2012;**81**(12):3965-3972.
21. Kim H, Kim JA, Son EJ, Youk JH. Quantitative assessment of shear-wave ultrasound elastography in thyroid nodules: diagnostic performance for predicting malignancy. *Eur Radiol*. 2013;**23**(9):2532-2537.

22. Park AY, Son EJ, Han K, Youk JH, Kim JA, Park CS. Shear wave elastography of thyroid nodules for the prediction of malignancy in a large scale study. *Eur J Radiol*. 2015;**84**(3):407-412.
23. Liu Z, Jing H, Han X, et al. Shear wave elastography combined with the thyroid imaging reporting and data system for malignancy risk stratification in thyroid nodules. *Oncotarget*. 2017;**8**(26):43406-43416.
24. Chang N, Zhang X, Wan W, Zhang C, Zhang X. The preciseness in diagnosing thyroid malignant nodules using shear-wave elastography. *Med Sci Monit*. 2018;**24**:671-677.
25. Bhatia KS, Tong CS, Cho CC, Yuen EH, Lee YY, Ahuja AT. Shear wave elastography of thyroid nodules in routine clinical practice: preliminary observations and utility for detecting malignancy. *Eur Radiol*. 2012;**22**(11):2397-2406.
26. Bardet S, Ciappuccini R, Pellot-Barakat C, et al. Shear wave elastography in thyroid nodules with indeterminate cytology: results of a prospective bicentric study. *Thyroid*. 2017;**27**(11):1441-1449.
27. Swan KZ, Nielsen VE, Bibby BM, Bonnema SJ. Is the reproducibility of shear wave elastography of thyroid nodules high enough for clinical use? A methodological study. *Clin Endocrinol (Oxf)*. 2017;**86**(4):606-613.
28. Anvari A, Dhyani M, Stephen AE, Samir AE. Reliability of shear-wave elastography estimates of the young modulus of tissue in follicular thyroid neoplasms. *AJR Am J Roentgenol*. 2016;**206**(3):609-616.
29. Yoo MH, Kim HJ, Choi IH, et al. Shear wave elasticity by tracing total nodule showed high reproducibility and concordance with fibrosis in thyroid cancer. *BMC Cancer*. 2020;**20**(1):118.
30. Jo VY, Stelow EB, Dustin SM, Hanley KZ. Malignancy risk for fine-needle aspiration of thyroid lesions according to the Bethesda System for Reporting Thyroid Cytopathology. *Am J Clin Pathol*. 2010;**134**(3):450-456.
31. DeMay RM. Follicular lesions of the thyroid. W(h)ither follicular carcinoma? *Am J Clin Pathol*. 2000;**114**(5):681-683.
32. Baloch ZW, Livolsi VA. Follicular-patterned lesions of the thyroid: the bane of the pathologist. *Am J Clin Pathol*. 2002;**117**(1):143-150.
33. Barr RG, Ferraioli G, Palmeri ML, et al. Elastography assessment of liver fibrosis: society of radiologists in ultrasound consensus conference statement. *Radiology*. 2015;**276**(3):845-861.
34. Yoo MH, Kim HJ, Choi IH, et al. Differential diagnosis of thyroid follicular neoplasm from nodular hyperplasia by shear wave elastography. *Soonchunhyang Med Sci*. 2019;**25**(1):10-19.
35. Yi KH, Park YJ, Koong S, et al. Revised Korean thyroid association management guidelines for patients with thyroid nodules and thyroid cancer. *Endocrinol Metab (Seoul)*. 2010;**25**(4):270-297.
36. Cibas ES, Ali SZ. The Bethesda system for reporting thyroid cytopathology. *Thyroid*. 2009;**19**(11):1159-1165.
37. Jung CK, Min HS, Park HJ, et al.; Korean Endocrine Pathology Thyroid Core Needle Biopsy Study Group. Pathology reporting of thyroid core needle biopsy: a proposal of the Korean endocrine pathology thyroid core needle biopsy study group. *J Pathol Transl Med*. 2015;**49**(4):288-299.
38. Hedrick W. *Technology for Diagnostic Sonography*. St Louis: Elsevier Mosby; 2013.
39. Sigrist RMS, Liau J, Kaffas AE, Chammas MC, Willmann JK. Ultrasound elastography: review of techniques and clinical applications. *Theranostics*. 2017;**7**(5):1303-1329.
40. Garra BS. Elastography: history, principles, and technique comparison. *Abdom Imaging*. 2015;**40**(4):680-697.
41. Rago T, Scutari M, Loiacono V, et al. Low elasticity of thyroid nodules on ultrasound elastography is correlated with malignancy, degree of fibrosis, and high expression of galectin-3 and fibronectin-1. *Thyroid*. 2017;**27**(1):103-110.
42. Yi L, Qiong W, Yan W, Youben F, Bing H. Correlation between ultrasound elastography and histologic characteristics of papillary thyroid carcinoma. *Sci Rep*. 2017;**7**:45042.
43. Fukuhara T, Matsuda E, Endo Y, et al. Impact of fibrotic tissue on shear wave velocity in thyroid: an ex vivo study with fresh thyroid specimens. *Biomed Res Int*. 2015;**2015**:569367.
44. Fukuhara T, Matsuda E, Endo Y, et al. Correlation between quantitative shear wave elastography and pathologic structures of thyroid lesions. *Ultrasound Med Biol*. 2015;**41**(9):2326-2332.
45. Yoo MH, Kim HJ, Choi IH, Yun S. *Shear Wave Elastography of Thyroid Nodules—A Guide to Differential Diagnosis by Means of the Stiffness Map*. Singapore: Springer Nature; 2021.
46. Yang W, Fananapazir G, LaRoy J, Wilson M, Campbell MJ. Can the American Thyroid Association, K-TIRADS and ACR-TIRADS ultrasound classification systems be used to predict malignancy in Bethesda category IV nodules? *Endocr Pract*. 2020;26(9):945-952.